The case of a southern European glacier that survived Roman and Medieval warm periods but is disappearing under recent warming

Ana Moreno[1], Miguel Bartolomé[2], Juan Ignacio López-Moreno[1], Jorge Pey[1,3], Juan Pablo Corella[4], Jordi García-Orellana[5,6], Carlos Sancho[Ŧ], María Leunda[7,8], Graciela Gil-Romera[9,1], Penélope González-Sampériz[1], Carlos Pérez-Mejías[10], Francisco Navarro[11], Jaime Otero-García[11], Javier Lapazaran[11], Esteban Alonso-González[1], Cristina Cid[12], Jerónimo López-Martínez[13], Belén Oliva-Urcia[13], Sérgio Henrique Faria[14,15], María José Sierra[4], Rocío Millán[4], Xavier Querol[16], Andrés Alastuey[16] and José M. García-Ruíz[1]

1. Departamento de Procesos Geoambientales y Cambio Global, Instituto Pirenaico de Ecología – CSIC, Zaragoza, Spain
2. Departamento de Geología, Museo de Ciencias Naturales - CSIC, Madrid, Spain
3. Fundación Aragonesa para la Investigación y el Desarrollo, ARAID, Zaragoza, Spain
4. CIEMAT — Environmental Department (DMA), Avenida Complutense 40, Madrid, Spain
5. Institut de Ciència i Tecnologia Ambientals, Universitat Autònoma de Barcelona, Barcelona, Spain
6. Departament de Física, Universitat Autònoma de Barcelona, Barcelona, Spain
7. Institute of Plant Sciences & Oeschger Centre for Climate Change Research, Bern, Switzerland
8. Swiss Federal Research Institute for Forest, Snow and Landscape Research WSL, Birmensdorf, Switzerland
9. Department of Ecology, Faculty of Biology, Philipps-Marburg University, Marburg, Germany
10. Institute of Global Environmental Change, Xi'an Jiaotong University, Xi'an, China
11. Departamento de Matemática Aplicada a las TIC, ETSI de Telecomunicación, Universidad Politécnica de Madrid, Madrid, Spain
12. Centro de Astrobiología – CSIC-INTA, Madrid, Spain
13. Departamento de Geología y Geoquímica, Facultad de Ciencias, Universidad Autónoma de Madrid, Madrid, Spain
14. Basque Centre for Climate Change (BC3), Leioa, Spain
15. IKERBASQUE, Basque Foundation for Science, Bilbao, Spain
16. Institute of Environmental Assessment and Water Research – CSIC, Barcelona, Spain

Ŧ Deceased

Corresponding author: Ana Moreno (amoreno@ipe.csic.es) ORCID: 0000-0001-7357-584X

Keywords

Pyrenees, mountain glacier, current global warming, Medieval Climate Anomaly, Monte Perdido

37 **Abstract**

38 Mountain glaciers have generally experienced an accelerated retreat over the last

39 three decades as a rapid response to current global warming. However, the response

40 to previous warm periods in the Holocene is not well-described for glaciers of the

41 southern Europe mountain ranges, such as the Pyrenees. The situation during the

42 Medieval Climate Anomaly (900-1300 CE) is particularly relevant since it is not certain

43 whether the southern European glaciers just experienced significant ice loss or

44 whether they actually disappeared. We present here the first chronological study of a

45 glacier located in the Central Pyrenees (NE Spain), the Monte Perdido Glacier (MPG),

46 carried out by different radiochronological techniques and a comparison with

47 geochemical proxies from neighboring paleoclimate records. The chronological model

48 evidences that the glacier endured during the Roman Period and the Medieval Climate

49 Anomaly. The lack of ice record dated from the last 600 years suggests that the ice

50 formed during the Little Ice Age has melted away. The analyses of several metals with

51 anthropogenic source that characterize the Industrial Period, such as Zn, Se, Cd, Hg

52 and Pb, reveal low concentrations in MPG ice, which provides further evidence about

53 the absence of the most recent ice. This study confirms the exceptional warming of the

54 last decades in the context of the last two millennia.

55

1. Introduction

Mountain glaciers are sensitive to climate variations on temporal scales from decades to centuries. It is well known that summer temperature and winter precipitation are the most important climate parameters influencing glacier mass balance (Oerlemans, 2001). Therefore, continuous records of past glacier size fluctuations provide valuable information about the timing and magnitude of Holocene climate shifts, which contributed to explain the characteristics and evolution of plant cover, human movements and land use (Solomina et al., 2015, 2016). Several glacier advances during the Neoglacial (which started around 6000-5000 years ago) have been identified and associated to sustained cooling periods across the North Atlantic (Wanner et al., 2011). The most recent period of global glacier expansion took place during the Little Ice Age (LIA), beginning in the 13th century and reaching a maximum between the 17th and 19th centuries (Solomina et al., 2016). Afterwards, most glaciers worldwide have retreated rapidly, as indicated by measurements of ice volume and ice-covered area, and this trend seems to have accelerated over the last three decades (Marzeion et al., 2014; Zemp et al., 2015, 2019).

Despite broad agreement on millennial-scale trends in global glacier fluctuations and Holocene climate variability (Davis et al., 2009; Solomina et al., 2015), regional variations are not so well constrained. The Pyrenees is a mountain range that currently hosts the majority of the southernmost glaciers in Europe. In this mountain chain there is a significant lack of knowledge about Holocene glacier fluctuations, with few evidences of Neoglacial advances (García-Ruiz et al., 2020). Based on Pyrenean tree-ring chronologies, summer temperatures during the Medieval Climate Anomaly (MCA, circa 900–1300 CE) were estimated to have been as warm as those of the 20th century (Büntgen et al., 2017), but no information is available on the glacier response to MCA warming. Conversely, glacier advance during the LIA is well constrained in the Pyrenees (García-Ruiz et al., 2014; González Trueba et al., 2008; Hughes, 2018; Oliva et al., 2018) and a significant deglaciation is also evident in recent times (López-Moreno et al., 2016; Rico et al., 2017). In particular, the period from the 1980s to present has been the most intense in terms of the number of glaciers that disappeared (from 39 inventoried Pyrenean glaciers in 1984 to 19 at present; Rico et al. 2017). Given the

87 small size of the Pyrenean glaciers and their current critical situation in the context of

88 global warming, we hypothesize that they could have disappeared completely during

89 warm periods such as the MCA.

90 This study is focused on Monte Perdido Glacier (MPG), located in the Marboré Cirque

91 in the Spanish Central Pyrenees. MPG is currently one of the best monitored small

92 glaciers (<0.5 km^2) worldwide (López-Moreno et al., 2016, 2019). Previous research

93 based on different ground-based remote sensing techniques has demonstrated a rapid

94 retreat of this glacier, with an average loss of ice thickness of about one meter per year

95 since 1981 (López-Moreno et al., 2016, 2019). This glacier is located in one of the few

96 valleys in the Pyrenees where information about Holocene glacier fluctuations exists.

97 The outermost moraine in Marboré Cirque was recently dated at 6900 ± 800 ^{36}Cl yr BP

98 (García-Ruiz et al., 2020), which is the oldest Holocene date available for glacial

99 deposits in Spain, and indicates a glacier advance during the Neoglacial period. Other

100 minor advances would have occurred in MPG prior to the LIA, as inferred from three

101 polished surfaces dated at 3500 ± 400, 2500 ± 300 and 1100 ± 100 ^{36}Cl yr BP (García-

102 Ruiz et al., 2020). Unfortunately, no information has been obtained on the glacier

103 response to Roman or MCA warming periods, remaining an open question whether

104 MPG just experienced significant ice loss or melted away totally. Most likely, the

105 voluminous moraine at the foot of the Monte Perdido Massif was deposited during the

106 LIA, indicating an important glacier advance. These results, together with the

107 evidences of long-term retreat from its LIA position indicated by pictures and

108 moraines, suggested that this glacier could disappear over the next few decades

109 (López-Moreno et al., 2016).

110 The present study aims to reconstruct the chronology of MPG ice sequence by using a

111 variety of dating techniques and the analysis of several proxies associated to

112 environmental and anthropogenic changes measured on a set of samples taken from a

113 transect. Such analyses will fill the existing knowledge gaps and answer the key

114 question of whether Pyrenean glaciers may have survived previous Holocene warm

115 periods.

116 **2. Study area**

117   The MPG (42°40′50″N; 0°02′15″E) is located in the Central Spanish Pyrenees, in the

118   Ordesa and Monte Perdido National Park (OMPNP) (Fig. 1). It currently consists of two

119   separate ice bodies, which were connected in the past. Both are north facing, lie on

120   structural flats beneath the main summit of the Monte Perdido Peak (3355 m a.s.l.)

121   and are surrounded by vertical cliffs of 500–800 m in height. At the base of the cliffs,

122   the Cinca River flows directly from the glacier and the surrounding slopes, and has

123   created a longitudinal west–east basin called the Marboré Cirque (5.8 km^2). This is the

124   area within the Pyrenees with the highest variety of recent morainic deposits (García-

125   Ruiz et al., 2014, 2020). Additionally, a 6 m thick sediment core obtained in 2011 from

126   a lake inside the cirque (Marboré Lake) provided valuable information from the last

127   14,600 years of the depositional evolution of the lake (Oliva-Urcia et al., 2018) and of

128   the regional variations in vegetation cover (Leunda et al., 2017). The Marboré Lake

129   (2595 m a.s.l.) is located in the Marboré or Tucarroya Cirque, in the northern face of

130   the Monte Perdido massif. The distance between the lake and the MPG is

131   approximately 1300 m and, therefore, both have been affected by similar

132   palaeoenvironmental conditions.

133   The total surface area of MPG in 2016 was 0.385 km^2, with an average decrease in

134   glacier ice thickness of 6.1 m during the period 2011 - 2017 (López-Moreno et al.,

135   2019). According to recent measurements of air temperature (July 2014 to October

136   2017), the 0 °C isotherm lies at 2945 m a.s.l., suggesting that the potential glacier

137   accumulation area is very small, even inexistent during warm years. The average

138   summer (June to September) temperature at the foot of the glacier from 2014 to 2017

139   has been of 7.3 °C (López-Moreno et al., 2019). No direct observations of precipitation

140   are available at the glacier location, but the maximum accumulated snow by late April

141   in the three available years (2014, 2015 and 2017, when no scanning limitations

142   occurred and the whole glacier was scanned) was 3.23 m, and field-measured average

143   snow density was 454 kg m^{-3}, indicating that total water equivalent during the main

144   accumulation period (October to April) could be equivalent to 1500 mm (López-

145   Moreno et al., 2019).

146   **3. Material and methods**

3.1. Ice sampling and storage

Ice sampling on MPG was carried out in September 2017 along a chrono-stratigraphical sequence covering from the oldest to the newest ice preserved in the glacier, following the isochronal layers that emerge in the ablation zone (Fig. 2A). Unfortunately, the extraction of vertical cores was not possible because the glacier does not currently meet any of the usual glacio-meteorological and topographical criteria required to obtain a preserved ice-core stratigraphy. The unfulfilled criteria include low temperatures to prevent water percolation or a large extension and flat surface topography to minimize the influence of glacier flow (Garzonio et al., 2018). Samples were collected in an area with no evidence of current ice movement (or very low), as confirmed by results from interferometric radar and GNSS measurements (López-Moreno et al., 2019). Due to the small size of this glacier, we expected the ice to be frozen to bedrock, and hence nearly stagnant, to become of substantial age, as indicated by previous studies in similar glaciers (Gabrielli et al., 2016; Haeberli et al., 2004). The sampling sector lies in the ablation zone of MPG and has been eroded to form a current steady slope of 20° where it is possible to observe the primary stratigraphy, marked by clear debris-rich layers. The distribution of these debris-rich layers is rather regular and extends laterally (Fig. 2B), as would be expected for the primary stratification resulting from the original deposition at surface of snow and debris. Therefore, these layers are considered isochrones, and confirm and facilitate the sampling along the slope, from the oldest to the newest ice preserved in the glacier.

We measured one-meter thickness using a Jacob's staff at each sampling point along the slope (Fig. 2B). The tilt of the ice layers was unclear but, since previous studies calculated about 30 m of ice thickness (López-Moreno et al., 2019), the ice layers are probably quite tilted downward as detailed in Fig. 2A. Once cleaned the most superficial ice (ca. 50 cm) to avoid possible ice formed recently, we recovered at every sampling position 3–4 small horizontal cores (6 cm in diameter and 25 cm in length) using a custom stainless-steel crown adaptor on a cordless power drill (Fig. 2C). Following this sampling procedure we recovered a total of 100 samples. The ice samples were stored in a freezer room at the IPE-CSIC in Zaragoza until they were

178   melted and analysed to obtain their chronology combining ^{210}Pb, ^{137}Cs and ^{14}C

179   techniques, and their geochemical composition in trace metals, such as Pb or Hg (see

180   below).

181   *3.2. Dating by ^{210}Pb and ^{137}Cs.*

182   The isotope ^{137}Cs, usually associated to the fallout from nuclear tests during the 1950s

183   and the 1960s, as well as the Chernobyl (1986) and Fukushima (2011) accidents, was

184   investigated by γ-spectrometry in five samples recovered towards the top of the MPG

185   chronological sequence (MP-61, MP-82, MP-97, MP-98, MP-100, Table 1). In addition,

186   ten samples were selected to perform a ^{210}Pb analysis as an independent dating

187   method to obtain the age model of approximately the last hundred years of glacier ice

188   (Eichler et al., 2000; Herren et al., 2013). These samples were selected also from the

189   top of the ice sequence to collect the younger ice (Table 2). Determination of ^{210}Pb

190   activities was accomplished through the measurement of its daughter nuclide, ^{210}Po,

191   by α-spectrometry following the methodology described in (Sanchez-Cabeza et al.,

192   1998) (Table 2).

193   *3.3. Dating by ^{14}C method.*

194   Sixteen accelerator mass spectrometry (AMS) ^{14}C dates from MPG ice were obtained

195   by combining bulk organic matter (9 samples), pollen concentrates (3 samples), bulk

196   sediment accumulated in filters (2 filters), and water-insoluble organic carbon (WIOC)

197   particles (2 samples) (Table 3). The procedure to select these samples was as follows:

198   (i) Using a binocular microscope [x10], we picked up organic particles for dating from

199   selected ice samples. However, the small size of the handpicked organic remains

200   prevented us from classifying them. As a result, we obtained 9 samples (MP-1, MP-42,

201   MP-48, MP-67, MP-68, MP-69, MP-70, MP-73, MP-100, Table 3) that were sent to the

202   Direct AMS laboratory (Seattle, USA) for dating. The selection of those nine samples

203   was based on the amount of debris found in the sample, once the ice was melted

204   (ii) Pollen concentrates were prepared from three samples (MP-30, MP-70 and MP-

205   100) to complete the previous set with the aim of replicating some of the results (MP-

206   70 and MP-100) and obtaining new dates (MP-30). Preparation followed the standard

palynological method, including a chemical treatment and mineral separation in heavy liquid (Thoulet: density 2.0; Moore et al., 1991). The effects of meltwater percolation on pollen in snow, firn and glacial ice are not fully understood and currently challenge the use of pollen in ice-core studies (Ewing et al., 2014). Just in few cases pollen has appeared as a potential dating material, when seasonal layers are preserved (Festi et al., 2017). Yet, pollen concentrates have been used in other type of archives with high success (Fletcher et al., 2017), opening the door to apply the same methodology here.

(iii) Two ice samples (MP-67 and MP-81), which appeared darker than others once melted, were filtered throughout a filtration line connected to a vacuum pump using 47 mm quartz fiber filters (PALL tissuquarzt 2500QAT-UP), parameterized at controlled conditions (temperature: 22 – 24 °C; relative humidity 25 – 35 %) and weighted twice in different days. Abundant material was obtained, but no control was made on the composition and amount of organic material versus other types of input. The three concentrated pollen samples and the two filters were dated at the same ^{14}C dating laboratory (Direct AMS, Seattle, USA) (Table 3).

(iv) Finally, two more samples were dated at the Laboratory of Environmental Chemistry, Paul Scherrer Institute (Switzerland) removing the outer part of the ice core segment for decontamination purposes (Jenk et al., 2009). Since organic fragments (plants, wood, insects) are rarely found in mountain glaciers, a new, complementary dating tool was recently developed based on extracting the microgram-amounts of the water-insoluble organic carbon (WIOC) fraction of carbonaceous aerosols embedded in the ice matrix for subsequent ^{14}C dating (Uglietti et al., 2016). These two samples, labelled as MP10m and MP59m at the WIOC facility (Table 3), were selected as the only ones with sufficient ice volume available.

Once the 16 radiocarbon ages were obtained, we converted them into calendar ages by using the CALIB 5.0.2 software, which uses the most updated dataset, INTCAL13 (Reimer et al., 2013) (Table 3). The median of the one-σ probability interval was selected for these dates, resulting in highly variable errors in the calendar ages obtained (from 30 years on the bulk organic samples to more than 200 years on pollen and WIOC samples). While the first method to select organic remains at the

microscope resulted the best option, the pollen concentration and filtering methods used to isolate organic matter to be dated by ^{14}C were, unfortunately, not successful. Finally, from the initial 16 dates, we had to discard seven according to the following criteria (see the "comments" column in Table 3):

- Sample MP-46 (D-AMS 025295) was the only one discarded from the nine initial bulk organic matter samples. We suspect that the very recent age obtained (1897 ± 20 CE, Table 3) is due to the sample contamination, since small plastic debris coming off from the painting used in the coring device were identified under the microscope.

- From the two WIOC-dated samples, one was discarded (MP10m) due to the low carbon content (5.3 μg), thus providing too inaccurate results (854 ± 721 CE, with an unacceptable large uncertainty). The other sample (MP59m), with higher organic carbon content (28.7 μg), was incorporated into the age model in spite of its error above 200 yr (1046 ± 242 CE).

- The three pollen concentrates provided unreliably old dates with very high errors, likely due to the small amount of pollen that we were able to concentrate (errors above 200 yr, Table 3). Obtaining old dates from pollen is a quite common problem not yet solved in the literature (Kilian et al., 2002).

- Similarly, we discarded the two filter samples MP-67 and MP-81 (D-AMS 029894 and D-AMS 033972, respectively). The material accumulated in the filters was a mixture of particles containing detrital carbonate eroded from Eocene limestones or supplied by Saharan dust, which was not removed and probably influenced the results incorporating allochthonous carbon to the samples.

Finally, nine dates were employed to infer the chronology of the MPG sequence. The depth–age model was created using a linear regression in the R package CLAM 2.2 (Blaauw, 2010; Blaauw et al., 2019).

3.4. Trace elements in soluble and insoluble material.

35 selected ice samples from the altitudinal transect were melted and filtered through a filtration ramp connected to a vacuum pump using 47 mm quartz fibre filters (PALL

tissuquarzt 2500QAT-UP). Filters were pre-heated at 250 °C and thereafter prepared in controlled conditions (temperature: 22 – 24 °C; relative humidity: 25 – 35 %) before and after filtration. Subsequently, they were weighted in two different days. Mass difference between blank and sampled filters was used to calculate the amount of insoluble material entrapped in ice samples. For every sample, an aliquot and a filter were obtained. From aliquots, anions and cations, as well as major and trace elements were determined. From filters, we determined major and trace elements, as well as organic and elemental carbon, following the method devised by Pey et al. (2013) (Table 4). Basically, an acidic digestion (HNO_3:HF:$HClO_4$) of half of each filter was conducted, driven to complete dryness, being the remaining material re-dissolved in HNO_3. Inductively coupled plasma mass spectrometry (ICP-MS) and inductively coupled plasma atomic emission spectroscopy (ICP-AES) were used to determine major and trace elements, respectively. From the other half of each filter, a 1.5 cm^2 section was used to determine Organic Carbon (OC) and Elemental Carbon (EC) concentrations by using a SUNSET thermo-optical analyzer, following the EUSAAR_2 temperature protocol. Table 1 also contains the Enrichment Factors (EFs), calculated as follows:

$$EF_{iCODD} = \frac{X_{iCODD}/Al_{CODD}}{X_{iUC}/Al_{UC}} \qquad EF_{iMPGID} = \frac{X_{iMPGID}/Al_{MPGID}}{X_{iUC}/Al_{UC}} \qquad EF_i = \frac{X_{iCODD}/Al_{CODD}}{X_{iMPGID}/Al_{MPGID}}$$

where EF_{iCODD} is the Al-normalised Enrichment Factor with respect to the Upper Crust (*UC*, Taylor and McLennan (1995)) of an *'i'* element in the current Ordesa's deposited dust (*CODD*); EF_{iMPGID} is the Al-normalised Enrichment Factor with respect to the *UC* of an *'i'* element in the current MPG ice dust (*MPGID*); and EF_i is the Al-normalised Enrichment Factor with respect to *CODD* of an *'i'* element in the *MPGID*.

Regarding the Pb/Al ratio, we carried out a normalization with Al in both, ice and lake records, to disentangle the anthropogenic lead variability from possible detrital inputs. Aluminium has been selected for normalization since this lithogenic element is immobile and abundant in carbonated watersheds (Corella et al., 2018).

3.5. Hg determination.

294   Total Hg concentration measurements were carried out in 21 selected samples by

295   Atomic Absorption Spectrophotometry using an Advance Mercury Analyzer (AMA 254,

296   LECO Company). This equipment is specifically designed for direct mercury

297   determination in solid and liquid samples without sample chemical pre-treatment.

298   Certified reference materials were used to determine the accuracy and precision of the

299   Hg measurements. These reference materials were ZC73027 (rice, 4.8 ± 0.8 µg kg^{-1})

300   and CRM051–050 (clay soil, 4.08 ± 0.09 mg kg^{-1}). The standard deviation (repeatability)

301   was ≤ 15 % and the relative uncertainty associated with the method (with a confidence

302   level of about 95 %) was ±20 %. All analyses were run at least three times. Total metal

303   concentrations were expressed in µg g^{-1} of dry weight sediment due to the low

304   amount detected.

305   **4. Results**

306   *4.1. Chronological model*

307   To date the ice sequence from MPG we compiled the results from ^{137}Cs, ^{210}Pb and ^{14}C

308   methods. First, it is remarkable the absence of ^{137}Cs in the five samples analyzed (Table

309   1). This implies that all samples are older than 60–65 years and therefore they were

310   not exposed to the atmosphere after 1950 CE. Another possibility that was discarded

311   upon obtaining ^{14}C dates, is that all samples were younger than 1950 CE. Similarly,

312   ^{210}Pb activity was also undetectable in most cases, except in three samples (MP-100,

313   MP-73 and MP-76) with concentrations above minimum detection activity (MDA; Table

314   2). These three samples contained a large amount of lithogenic particulate material

315   from atmospheric dust or ash deposits, likely causing the observed values. Thus, the

316   absence of ^{210}Pb activity in the analysed samples suggests that MPG ice samples were

317   very likely older than 100 years and the ^{210}Pb had completely decayed. We then built

318   up the proposed MPG chronology using only AMS ^{14}C dating.

319   Regarding ^{14}C dating, we took most of the ice samples for dating in sections where

320   dark debris layers alternated every ca. 5 m with cleaner and clearer ice (Fig. 2). The

321   debris-rich layers were composed of detrital, silty-sandy size deposits, likely coming

322   from wind-blown particles (e.g. black carbon-rich particles, dust) and from erosive

323   processes of the limestone catchment, including the fall of gravel-sized particles from

324 the surrounding cliffs. These debris-rich layers do not have a subglacially derived origin

325 since they are observed all along the sample profile and large accumulation of debris

326 or pinnacles, both characteristics of subglacially derived glacier till, were not found in

327 MPG. These debris layers contain more organic remains than those formed by clear

328 ice, making them ideal spots to find datable remains.

329 Interestingly, the frequency of debris layers increases towards the top of the glacier

330 sequence. We consider the accumulation of debris layers to be indicative of reduced

331 ice accumulation and dominance of ablation periods. In such situations, the detrital

332 and organic material concentrates as the ice melts, giving its characteristic dark colour

333 to the ice layers. The major concentration of such layers occurred among samples MP-

334 67 and MP-73 (Table 3), thus suggesting the dominance of ablation processes.

335 Therefore, we run the depth–age model setting a hiatus at 73 m depth, where we

336 think an interruption in the ice accumulation was produced. Finally, as explained in the

337 methods section, the age-model was constructed with 9 of the initially dated 16

338 samples (Table 3). Given the scattered depths at which dates concentrate, we chose to

339 perform a non-smooth, linear regression for preventing any model over-fitting and a

340 spurious age–depth relationship (Fig. 3). Full details on how the model was performed

341 and a reproducible workflow with the current chronological dataset are stored at

342 https://zenodo.org/record/3886911.

343 4.2. Trace elements

344 We have used the averaged concentration values of major and trace elements

345 currently obtained at a monitoring station located at OMPNP (8 km away from the

346 MPG, at 1190 m a.s.l.), where deposited atmospheric particulate matter is sampled

347 monthly (Table 4) (Pey et al., 2020). Interestingly, the elements that are abundant

348 nowadays in the Ordesa station are not so frequent in the ice from MPG. Indicators

349 such as organic carbon, Zn, Se and Cd concentrations, all of which are potential proxies

350 of current anthropogenic emissions, are much higher in the samples from Ordesa,

351 which are representative of today's atmosphere, than in the ice samples from the

352 MPG. The low concentration of these elements in MPG samples could indicate their

353 disappearance from glacier surface layers due to its continuous melting. This supports

our suggested age model (Fig. 3), in which ages from the Industrial Period are not recorded. Conversely, the Al-normalised enrichment factor (EF) of Ti, Mn, Cr, Co, Ni, Cu and Pb, elements linked to the natural fraction (dust deposition, lithogenic elements) and mining activities (Corella et al., 2018), are more abundant in the MPG ice samples than in the present-day Ordesa aerosols (Table 4). From them, Cu and Pb were markedly enriched (by a factor >6) in the MPG ice samples compared with the current deposited aerosols in Ordesa station.

5. Discussion

5.1. Dating Monte Perdido Glacier ice sequence

Dating the ice from non-polar glaciers is challenging and often problematic as annual layer counting is precluded due to periods without net accumulation, and to common ice deformation caused by glacier flow (Bohleber, 2019; Festi et al., 2017). We have constrained the age model of MPG ice using nine ^{14}C absolute dating from different materials (Table 3), the absence of [137]C and ^{210}Pb in surface ice samples and integrating in the chronology the characteristics of the ice stratigraphy, such as the presence of dark debris-rich layers.

The age-depth model obtained indicates the presence of ice since 2000 years ago and allows distinguishing three main periods for MPG (Fig. 3). Period I was an accumulation period from 0 to 700 CE. Period II represents an ablation-dominated phase from 700 to 1200 CE, which corresponds to the dark-rich layer interval where more dates are concentrated. Period III corresponds to a new accumulation period from 1200 to 1400 CE. This period agrees well with an increase in cold season (Oct–May) heavy rainfall events in the Southern Central Pyrenees between 1164 – 1414 CE (Corella et al., 2016) that most likely resulted on higher snow accumulation at high elevation areas, leading to a net accumulation in MPG. Finally, no ice formed during, at least, the last 600 years has been found today in MPG. This indicates that the LIA ice has been melted away, pointing to an intense ablation period since 1850 CE. The MPG age model is supported by, first, a quantitative comparison with present-day atmospheric particulate matter (Table 4) and, second, by the comparison with the paleoenvironmental sequence of

383 the Marboré Lake for the last 2000 years (Corella et al., 2021; Oliva-Urcia et al., 2018)

384 (Fig. 4).

385 Present-day aerosols in the studied region are well-recorded in Ordesa site (Pey et al.,

386 2020). Following previous studies on present-day atmospheric particulate matter

387 composition from natural, urban or industrial areas (Querol et al., 2007), the values of

388 some elemental ratios (e.g., Cu/Mn, As/Se, Pb/Zn) help to determine the origin of the

389 particulate matter accumulated today. The Ordesa site can accordingly be mostly

390 defined as remote in terms of atmospheric deposition ("rural background") while the

391 average composition of MPG ice samples could be defined as a site under the influence

392 of Cu mining and smelting activities, due to the high values of the Cu/Mn, As/Se and

393 Pb/Zn ratios. It is noteworthy that Cu, Ag, and Pb mining and smelting have been

394 historically documented in Bielsa valley during pre-industrial times (Callén, 1996).

395 Indeed, MPG is only 7 km east from some of the largest lead and silver ore deposits in

396 the Central Pyrenees (historical mines of Parzán). The impact of ancient environmental

397 pollution in high alpine environments is archived in the lacustrine sequence of the

398 neighbouring Marboré Lake, providing first evidences of long-range transport of trace

399 metals from historical metal mining and smelting activities during the Roman Period

400 (RP) (Corella et al., 2018, 2021). Similar ice core records from the Alps have also

401 demonstrated the suitability of glacier ice to record local and regional mining and

402 smelting activities during RP and pre-Roman times (More et al., 2017; Preunkert et al.,

403 2019). Even if the enrichment of trace elements in MPG ice record may correspond to

404 mining activities during ancient times, the different altitude of MPG glacier with

405 respect to records from Alpine glaciers where such activities were recorded (> 4000m

406 a.s.l.), together with the likely processes of redistribution of chemical impurities due to

407 percolation (Pohjola et al., 2002), prevents a firm interpretation of the origin of these

408 elements.

409 On the other hand, the comparison of Pb/Al ratios from the independently dated

410 records of Marboré Lake and MPG provides further support to the obtained glacier

411 chronology (Fig. 4). In particular, the lack of a Pb/Al peak characterizing the Industrial

412 Period in the upper sequence of the MPG confirms the absence of the last two

413 centuries in MPG ice record, in agreement with the ^{210}Pb and ^{137}Cs analyses. Similarly,

the Hg concentration in the glacier is very stable throughout the ice sequence (Fig.4). Hg concentrations in other ice core records show an increase during the onset of Industrialization at 1800 CE with maximum values typically 3–10 times higher than preindustrial values (Cooke et al., 2020). In Marboré Lake, the Hg increase occurred over the last 500 years associated to the maximum activity in the Spanish Almadén mines during the Colonial Period (Corella et al., 2021). Again, these results, lacking an expected increase in Hg levels, support the age model from the MPG record where the last six centuries of ice deposition are missing.

5.2. Evolution of the Monte Perdido glacier over the last 2000 years

The analyzed ice from MPG provides valuable information about the evolution of the glacier during the last two millennia, which deserves consideration in the regional context. Based on published results, the oldest paleoclimatic information in the Marboré Cirque comes from the Marboré Lake, since no glacier deposits corresponding to the Late Pleistocene have been found in the cirque (García-Ruiz et al., 2014). There is sedimentological evidence that the Marboré Lake was already ice-free at least since the onset of the Bølling period (Greenland Interstadial-1, 14,600 yr BP), when clastic sediments were deposited in the lake basin (Leunda et al., 2017; Oliva-Urcia et al., 2018). This is coherent with the nearby La Larri juxta-glacial sequence which showed that the main Pineta glacier had already retreated further up in the headwater by 11 kyr BP (Salazar et al., 2013). In fact, glaciological studies performed in the Central Pyrenees confirm the sudden retreat of glaciers during the Bølling period, when they were reduced to small ice tongues or cirque glaciers (Palacios et al., 2017). The next piece of information comes from the outermost moraine that was dated at 6900 ± 800 [36]Cl yr BP (García-Ruiz et al., 2020), corresponding to the Neoglacial advance, a cold period identified in the sediments of Marbore Lake (Leunda et al., 2017). Other minor advances would have occurred in MPG prior to the LIA, as inferred from three polished surfaces dated at 3500 ± 400, 2500 ± 300 and 1100 ± 100 [36]Cl yr BP (García-Ruiz et al., 2020).

With the new chronology of the MPG record, we can ascertain that MPG has persisted at least since the RP (ca. 2000 years ago). At that time, which is a well-known warm

period in the Iberian Peninsula as recorded in both continental (Martín-Puertas et al., 2010; Morellón et al., 2009) and marine sequences (Cisneros et al., 2016; Margaritelli et al., 2020), the glacier was still present, but probably smaller than during previous Neoglacial times (Fig. 5B). This situation probably continued during the following cold period, the Dark Ages (DA, Fig 5C) when the glacier advanced as indicated by the polished surface dated at 1100 ± 100 ^{36}Cl yr BP (García-Ruiz et al., 2020). In the Alps, reconstructions based on dating trees found within and at the edge of glacier forefields have revealed a minimum glacier extent during the Iron Age and the RP (Holzhauser et al., 2005), when glaciers were estimated to be smaller than during the 1920s (Ivy-Ochs et al., 2009). Afterwards, in the late RP and the early Middle Ages numerous glaciers in the Alps advanced during the DA, also known as the Göschener II oscillation (Holzhauser et al., 2005).

The MCA (900–1300 CE) is the most recent preindustrial warm era in Europe (Mann et al., 2009). For instance, in the Alps, a general glacier retreat has been observed during this period, mainly associated with a decline in precipitation (Holzhauser et al., 2005). According to the age-depth model, the MPG experienced a spectacular retreat (Fig. 5D), including the complete melting of some minor glaciers in the Marboré Cirque (García-Ruiz et al., 2020). Nevertheless, during the MCA part of MPG was preserved, as we find ice from 0 to 700 CE. No doubt the ice loss was significant, as evidenced by the accumulation of dark strata over a long time interval (600 – 1200 CE) (Fig.3). On this basis, we propose that the MPG was dominated by ablation processes during the MCA, leading to considerable ice loss as deduced from just six meters of ice remaining from this period (blue horizontal line, Fig. 3). It is evident that at the end of the MCA the MPG still preserved ice from the RP and the first half of the DA (Fig. 5D). It is difficult to assure if Neoglacial basal ice is still present in MPG since no ice sample was dated with Neoglacial age or even older. Still, Neoglacial ice can remain in the glacier base without being exposed by the slope where sampling procedures were carried out.

Over such a diminished MCA glacier, ice started to accumulate again at a rapid rate during the LIA (1300 – 1850 CE). In most cases, the LIA was the period when mountain glaciers recorded their maximum Holocene extent (Solomina et al., 2016), with remarkable advances in the alpine glaciers (Ivy-Ochs et al., 2009). From a large variety

of proxies, several warm and cold periods have been identified in the Iberian Peninsula during the LIA (Oliva et al., 2018). In the Marboré Cirque two generations of LIA moraines have been mapped (García-Ruiz et al., 2014), whose emplacement coincided with the coldest LIA phases, i.e. 1620 - 1715 CE, when the Pyrenean glaciers recorded their maximum extent of the last two millennia, and at some time between 1820 - 1840 CE, when a rapid advance of the ice mass moved over the large moraine leaving parallel ridges and furrows, so-called flutes, as signs of erosion (García-Ruiz et al., 2020; Serrano and Martín-Moreno, 2018). These two cold phases are very well identified in the Marboré Cirque and were confirmed by the study of the altitudinal fluctuations of the timberline in the neighboring Escuaín Valley (Camarero et al., 2015). In fact, according to the map of Schrader from 1874 CE and other historical sources, the MPG made direct contact with the large moraine in the second half of the 19th century (García-Ruiz et al., 2014). Despite the fact that the MPG would have covered an area of 5.56 km^2 at the end of the LIA (in 1894 (González Trueba et al., 2008), Fig. 5E), there is no record today of ice accumulated during the LIA, except for a few meters at the top of the sequence corresponding to about 1400 CE. This means that more than 600 years of ice accumulation have been lost associated to the warming after ca. 1850 CE. This situation is not so common in the Alps, where ice from the LIA, and even from the last two centuries, is still preserved in many studied cold glaciers (Eichler et al., 2000; Gabrielli et al., 2016; Gäggeler et al., 1983; Preunkert et al., 2019).

Today the MPG is divided in two small ice bodies that together cover just 0.38 km^2 (López-Moreno et al., 2016, Fig. 5F). Comparing the MPG extent at the end of the LIA (ca. 1850 CE), as given by the moraine location, and today's extent, more than 5 km^2 of MPG would have disappeared, thus indicating that the last 150 years have likely been the period with the largest glacier melting over the last 2000 years.

5. Conclusions

This study presents for the first time a continuous chronological model of a remaining small glacier in the Pyrenees, reconstructed from a set of ^{14}C dates on different organic remains, and supported by measurements of current atmospheric deposition and comparison with a nearby lake sequence (Marboré Lake). The ice sequence from MPG

covers the last 2000 years, allowing the identification of cold time periods of growing glaciers and warm time periods of ice loss. We demonstrate that the glacier was active during the RP, a well-known warm period in the Iberian Peninsula. During the MCA, the MPG experienced a spectacular retreat marked by the presence of dark debris layers indicative of successive years when ablation processes predominated. The LIA was a period of glacier growth but is not recorded today in the ice from MPG, since more than 600 years of ice accumulation have been lost associated to the warming after the end of the LIA, ca. 1850 CE. This evidence from the age-depth model is supported by the lack of anthropogenic indicators usually associated to the Industrial Era abundant today in current atmospheric deposition in a nearby site. Additionally, both Hg concentration and Pb/Al ratio appear much higher in the Marboré Lake sediments, whereas the MPG record does not reflect their anthropogenic increase.

Comparing the present-day glacier situation with that of previous warm intervals, such as the RP or the MCA, we conclude that the MPG is nowadays greatly reduced in area and volume. Additionally, the recent rate of ice-mass loss is definitely more rapid than that of the four centuries spanned by the MCA, thus suggesting that present day warming in the Pyrenees is faster and more intense than in any previous warm phase of the last 2000 years. Under the current climatic conditions, it is reasonable to expect the disappearance of this glacier, as well as other glaciers in the Pyrenees and in Southern Europe, over the next few decades.

6. Data availability

The input data file for CLAM as well as the output results are stored in the open repository Zenodo (https://zenodo.org/record/3886911). The rest of data are given in the paper Tables.

7. Author contributions

The paper was conceived by A.M., M.B., C.S. and J.I.L-M. together with F.N., J.O-G., J.L., P.G-S., C.C., J.L-M., B.O-U, S.H.F and J.G-R. who contributed to design and develop this research project (PaleoICE). F.N., C.P., M.L., E.A. participated during field work to recover the samples; A.M., M.B. and M.L. prepared the samples for ^{14}C dating; J.G.O.

carried out the ^{210}Pb and ^{137}Cs analyses; J.P., X.Q. and A.A. provided the geochemical data from Ordesa site and MPG; J.P.C., M.J.S. and R.M. provided the Hg data from Marboré Lake and MPG; and G.G.-R. built the age depth-model. All authors contributed to discuss and interpret the data and to the writing of the original and revised version of this paper.

8. Competing interest

The authors declare that they have no conflict of interest.

9. Acknowledgements

The Spanish Agencia Estatal de Investigación (AEI – Spain) and the European Funds for Regional Development (FEDER – European Union) are gratefully acknowledged for financial support through PaleoICE EXPLORA project (CGL2015-72167-EXP), CGL2015-68993-R, CGL2015-69160-R and CTM2017-84441-R projects (AEI/FEDER, UE) and through the iMechPro RETOS project (RTI2018-100696-B-I00). S.H.F. and J.G.-O. acknowledge support by the Spanish Government through María de Maeztu excellence accreditation 2018-2022 ref MDM-2017-0714 and ref CEX-2019-000940-M, respectively. M.B. is supported by postdoctoral fellowship Juan de la Cierva-Formación program provided by the Spanish Ministry of Science, Innovation and Universities (ref.: FJCI-2017-34235063753). The authors are grateful to Eduardo Bartolomé and José Esteban Lozano for their help manufacturing parts of the coring devices and to the support provided by the Dirección General de Conservación del Medio Natural (Government of Aragón) and by the staff of the Ordesa and Monte Perdido National Park during our field campaigns. This study contributes to the work carried out by the GA research group Procesos Geoambientales y Cambio Global (ref E02-20R) and MERS research group 2017 SGR 1588.

10. References

Blaauw, M.: Methods and code for 'classical' age-modelling of radiocarbon sequences, Quaternary Geochronology, 5(5), 512–518, doi:10.1016/j.quageo.2010.01.002, 2010.

Blaauw, M., Christen, J. A., Vázquez, J. E. and Goring, S.: clam: Classical Age-Depth Modelling of Cores from Deposits. CRAN 2019, [online] Available from: https://CRAN.R-project.org/package=clam, 2019.

564 Bohleber, P.: Alpine Ice Cores as Climate and Environmental Archives, Oxford Research
565 Encyclopedia of Climate Science, doi:10.1093/acrefore/9780190228620.013.743, 2019.

566 Büntgen, U., Krusic, P. J., Verstege, A., Sangüesa-Barreda, G., Wagner, S., Camarero, J. J.,
567 Ljungqvist, F. C., Zorita, E., Oppenheimer, C., Konter, O., Tegel, W., Gärtner, H., Cherubini, P.,
568 Reinig, F. and Esper, J.: New Tree-Ring Evidence from the Pyrenees Reveals Western
569 Mediterranean Climate Variability since Medieval Times, J. Climate, 30(14), 5295–5318,
570 doi:10.1175/JCLI-D-16-0526.1, 2017.

571 Callén, J. J. N.: El proceso sidero-metalúrgico altoaragonés: los valles de Bielsa y Gistain en la
572 Edad Moderna (1565-1800), Llull: Revista de la Sociedad Española de Historia de las Ciencias y
573 de las Técnicas, 19(37), 471–508, 1996.

574 Camarero, J. J., García-Ruiz, J. M., Sangüesa-Barreda, G., Galván, J. D., Alla, A. Q., Sanjuán, Y.,
575 Beguería, S. and Gutiérrez, E.: Recent and Intense Dynamics in a Formerly Static Pyrenean
576 Treeline, Arctic, Antarctic, and Alpine Research, 47(4), 773–783, doi:10.1657/AAAR0015-001,
577 2015.

578 Cisneros, M., Cacho, I., Frigola, J., Canals, M., Masqué, P., Martrat, B., Casado, M., Grimalt, J.
579 O., Pena, L. D., Margaritelli, G. and Lirer, F.: Sea surface temperature variability in the central-
580 western Mediterranean Sea during the last 2700 years: a multi-proxy and multi-record
581 approach, Clim. Past, 12(4), 849–869, doi:10.5194/cp-12-849-2016, 2016.

582 Cooke, C. A., Martínez-Cortizas, A., Bindler, R. and Sexauer Gustin, M.: Environmental archives
583 of atmospheric Hg deposition – A review, Science of The Total Environment, 709, 134800,
584 doi:10.1016/j.scitotenv.2019.134800, 2020.

585 Corella, J. P., Valero-Garcés, B. L., Vicente- Serrano, S. M., Brauer, A. and Benito, G.: Three
586 millennia of heavy rainfalls in Western Mediterranean: frequency, seasonality and atmospheric
587 drivers, Scientific Reports, 6(1), doi:10.1038/srep38206, 2016.

588 Corella, J. P., Saiz-Lopez, A., Sierra, M. J., Mata, M. P., Millán, R., Morellón, M., Cuevas, C. A.,
589 Moreno, A. and Valero-Garcés, B. L.: Trace metal enrichment during the Industrial Period
590 recorded across an altitudinal transect in the Southern Central Pyrenees, Science of The Total
591 Environment, 645, 761–772, doi:10.1016/j.scitotenv.2018.07.160, 2018.

592 Corella, J. P., Sierra, M. J., Garralón, A., Millán, R., Rodríguez-Alonso, J., Mata, M. P., de Vera, A.
593 V., Moreno, A., González-Sampériz, P., Duval, B., Amouroux, D., Vivez, P., Cuevas, C. A., Adame,
594 J. A., Wilhelm, B., Saiz-Lopez, A. and Valero-Garcés, B. L.: Recent and historical pollution legacy
595 in high altitude Lake Marboré (Central Pyrenees): A record of mining and smelting since pre-
596 Roman times in the Iberian Peninsula, Science of The Total Environment, 751, 141557,
597 doi:10.1016/j.scitotenv.2020.141557, 2021.

598 Davis, P. T., Menounos, B. and Osborn, G.: Holocene and latest Pleistocene alpine glacier
599 fluctuations: a global perspective, Quaternary Science Reviews, 28(21–22), 2021–2033,
600 doi:10.1016/j.quascirev.2009.05.020, 2009.

601 Eichler, A., Schwikowski, M., Gäggeler, H. W., Furrer, V., Synal, H.-A., Beer, J., Saurer, M. and
602 Funk, M.: Glaciochemical dating of an ice core from upper Grenzgletscher (4200 m a.s.l.),
603 Journal of Glaciology, 46(154), 507–515, doi:10.3189/172756500781833098, 2000.

Ewing, M. E., Reese, C. A. and Nolan, M. A.: The potential effects of percolating snowmelt on palynological records from firn and glacier ice, Journal of Glaciology, 60(222), 661–669, doi:10.3189/2014JoG13J158, 2014.

Festi, D., Carturan, L., Kofler, W., dalla Fontana, G., de Blasi, F., Cazorzi, F., Bucher, E., Mair, V., Gabrielli, P. and Oeggl, K.: Linking pollen deposition and snow accumulation on the Alto dell'Ortles glacier (South Tyrol, Italy) for sub-seasonal dating of a firn temperate core, The Cryosphere, 11(2), 937–948, doi:10.5194/tc-11-937-2017, 2017.

Fletcher, W. J., Zielhofer, C., Mischke, S., Bryant, C., Xu, X. and Fink, D.: AMS radiocarbon dating of pollen concentrates in a karstic lake system, Quaternary Geochronology, 39, 112–123, doi:10.1016/j.quageo.2017.02.006, 2017.

Gabrielli, P., Barbante, C., Bertagna, G., Bertó, M., Binder, D., Carton, A., Carturan, L., Cazorzi, F., Cozzi, G., Dalla Fontana, G., Davis, M., De Blasi, F., Dinale, R., Dragà, G., Dreossi, G., Festi, D., Frezzotti, M., Gabrieli, J., Galos, S. P., Ginot, P., Heidenwolf, P., Jenk, T. M., Kehrwald, N., Kenny, D., Magand, O., Mair, V., Mikhalenko, V., Lin, P. N., Oeggl, K., Piffer, G., Rinaldi, M., Schotterer, U., Schwikowski, M., Seppi, R., Spolaor, A., Stenni, B., Tonidandel, D., Uglietti, C., Zagorodnov, V., Zanoner, T. and Zennaro, P.: Age of the Mt. Ortles ice cores, the Tyrolean Iceman and glaciation of the highest summit of South Tyrol since the Northern Hemisphere Climatic Optimum, The Cryosphere, 10(6), 2779–2797, doi:10.5194/tc-10-2779-2016, 2016.

Gäggeler, H., Gunten, H. R. von, Rössler, E., Oeschger, H. and Schotterer, U.: 210Pb-Dating of Cold Alpine Firn/Ice Cores From Colle Gnifetti, Switzerland, Journal of Glaciology, 29(101), 165–177, doi:10.1017/S0022143000005220, 1983.

García-Ruiz, J. M., Palacios, D., Andrés, N. de, Valero-Garcés, B. L., López-Moreno, J. I. and Sanjuán, Y.: Holocene and 'Little Ice Age' glacial activity in the Marboré Cirque, Monte Perdido Massif, Central Spanish Pyrenees, The Holocene, 0959683614544053, doi:10.1177/0959683614544053, 2014.

García-Ruiz, J. M., Palacios, D., Andrés, N. and López-Moreno, J. I.: Neoglaciation in the Spanish Pyrenees: a multiproxy challenge, Med. Geosc. Rev., 2(1), 21–36, doi:10.1007/s42990-020-00022-9, 2020.

Garzonio, R., Di Mauro, B., Strigaro, D., Rossini, M., Colombo, R., De Amicis, M. and Maggi, V.: Mapping the suitability for ice-core drilling of glaciers in the European Alps and the Asian High Mountains, J. Glaciol., 64(243), 12–26, doi:10.1017/jog.2017.75, 2018.

González Trueba, J. J., Moreno, R. M., Martínez de Pisón, E. and Serrano, E.: `Little Ice Age' glaciation and current glaciers in the Iberian Peninsula, The Holocene, 18(4), 551–568, doi:10.1177/0959683608089209, 2008.

Haeberli, W., Frauenfelder, R., Kääb, A. and Wagner, S.: Characteristics and potential climatic significance of "miniature ice caps" (crest- and cornice-type low-altitude ice archives), Journal of Glaciology, 50(168), 129–136, doi:10.3189/172756504781830330, 2004.

Herren, P.-A., Eichler, A., Machguth, H., Papina, T., Tobler, L., Zapf, A. and Schwikowski, M.: The onset of Neoglaciation 6000 years ago in western Mongolia revealed by an ice core from the Tsambagarav mountain range, Quaternary Science Reviews, 69, 59–68, doi:10.1016/j.quascirev.2013.02.025, 2013.

Holzhauser, H., Magny, M. and Zumbühl, H. J.: Glacier and lake-level variations in west-central Europe over the last 3500 years, The Holocene, 15(6), 789–801, 2005.

Hughes, P. D.: Little Ice Age glaciers and climate in the Mediterranean mountains: a new analysis, CIG, 44(1), 15, doi:10.18172/cig.3362, 2018.

Ivy-Ochs, S., Kerschner, H., Maisch, M., Christl, M., Kubik, P. W. and Schlüchter, C.: Latest Pleistocene and Holocene glacier variations in the European Alps, Quaternary Science Reviews, 28(21–22), 2137–2149, doi:10.1016/j.quascirev.2009.03.009, 2009.

Jenk, T. M., Szidat, S., Bolius, D., Sigl, M., Gäggeler, H. W., Wacker, L., Ruff, M., Barbante, C., Boutron, C. F. and Schwikowski, M.: A novel radiocarbon dating technique applied to an ice core from the Alps indicating late Pleistocene ages, Journal of Geophysical Research: Atmospheres, 114(D14), doi:10.1029/2009JD011860, 2009.

Kilian, M. R., van der Plicht, J., van Geel, B. and Goslar, T.: Problematic 14C-AMS dates of pollen concentrates from Lake Gosciaz (Poland), Quaternary International, 88(1), 21–26, doi:10.1016/S1040-6182(01)00070-2, 2002.

Leunda, M., González-Sampériz, P., Gil-Romera, G., Aranbarri, J., Moreno, A., Oliva-Urcia, B., Sevilla-Callejo, M. and Valero-Garcés, B.: The Late-Glacial and Holocene Marboré Lake sequence (2612m a.s.l., Central Pyrenees, Spain): Testing high altitude sites sensitivity to millennial scale vegetation and climate variability, Global and Planetary Change, 157, 214–231, doi:10.1016/j.gloplacha.2017.08.008, 2017.

López-Moreno, J. I., Revuelto, J., Rico, I., Chueca-Cía, J., Julián, A., Serreta, A., Serrano, E., Vicente-Serrano, S. M., Azorin-Molina, C., Alonso-González, E. and García-Ruiz, J. M.: Thinning of the Monte Perdido Glacier in the Spanish Pyrenees since 1981, The Cryosphere, 10(2), 681–694, doi:10.5194/tc-10-681-2016, 2016.

López-Moreno, J. I., Alonso-González, E., Monserrat, O., Del Río, L. M., Otero, J., Lapazaran, J., Luzi, G., Dematteis, N., Serreta, A., Rico, I., Serrano-Cañadas, E., Bartolomé, M., Moreno, A., Buisan, S. and Revuelto, J.: Ground-based remote-sensing techniques for diagnosis of the current state and recent evolution of the Monte Perdido Glacier, Spanish Pyrenees, J. Glaciol., 65(249), 85–100, doi:10.1017/jog.2018.96, 2019.

Mann, M. E., Zhang, Z., Rutherford, S., Bradley, R. S., Hughes, M. K., Shindell, D., Ammann, C., Faluvegi, G. and Ni, F.: Global Signatures and Dynamical Origins of the Little Ice Age and Medieval Climate Anomaly, Science, 326(5957), 1256–1260, 2009.

Margaritelli, G., Cacho, I., Català, A., Barra, M., Bellucci, L. G., Lubritto, C., Rettori, R. and Lirer, F.: Persistent warm Mediterranean surface waters during the Roman period, Scientific Reports, 10(1), 10431, doi:10.1038/s41598-020-67281-2, 2020.

Martín-Puertas, C., Jiménez-Espejo, F., Martínez-Ruiz, F., Nieto-Moreno, V., Rodrigo, M., Mata, M. P. and Valero-Garcés, B. L.: Late Holocene climate variability in the southwestern Mediterranean region: an integrated marine and terrestrial geochemical approach, Clim. Past, 6(6), 807–816, doi:10.5194/cp-6-807-2010, 2010.

Marzeion, B., Cogley, J. G., Richter, K. and Parkes, D.: Attribution of global glacier mass loss to anthropogenic and natural causes, Science, 345(6199), 919–921, doi:10.1126/science.1254702, 2014.

686   Moore, P. D., Webb, J. A. and Collinson, M. E.: Pollen Analysis, Second., Blackwell Scientific
687   Publications., 1991.

688   More, A. F., Spaulding, N. E., Bohleber, P., Handley, M. J., Hoffmann, H., Korotkikh, E. V.,
689   Kurbatov, A. V., Loveluck, C. P., Sneed, S. B., McCormick, M. and Mayewski, P. A.: Next-
690   generation ice core technology reveals true minimum natural levels of lead (Pb) in the
691   atmosphere: Insights from the Black Death, GeoHealth, 1(4), 211–219,
692   doi:10.1002/2017GH000064, 2017.

693   Morellón, M., Valero-Garcés, B., Vegas-Vilarrúbia, T., González-Sampériz, P., Romero, Ó.,
694   Delgado-Huertas, A., Mata, P., Moreno, A., Rico, M. and Corella, J. P.: Lateglacial and Holocene
695   palaeohydrology in the western Mediterranean region: The Lake Estanya record (NE Spain),
696   Quaternary Science Reviews, 28(25–26), 2582–2599, 2009.

697   Oerlemans, J.: Glaciers and Climate Change, CRC Press., 2001.

698   Oliva, M., Ruiz-Fernández, J., Barriendos, M., Benito, G., Cuadrat, J. M., Domínguez-Castro, F.,
699   García-Ruiz, J. M., Giralt, S., Gómez-Ortiz, A., Hernández, A., López-Costas, O., López-Moreno,
700   J. I., López-Sáez, J. A., Martínez-Cortizas, A., Moreno, A., Prohom, M., Saz, M. A., Serrano, E.,
701   Tejedor, E., Trigo, R., Valero-Garcés, B. and Vicente-Serrano, S. M.: The Little Ice Age in Iberian
702   mountains, Earth-Science Reviews, 177, 175–208, doi:10.1016/j.earscirev.2017.11.010, 2018.

703   Oliva-Urcia, B., Moreno, A., Leunda, M., Valero-Garcés, B., González-Sampériz, P., Gil-Romera,
704   G., Mata, M. P. and Group, H.: Last deglaciation and Holocene environmental change at high
705   altitude in the Pyrenees: the geochemical and paleomagnetic record from Marboré Lake (N
706   Spain), J Paleolimnol, 59(3), 349–371, doi:10.1007/s10933-017-0013-9, 2018.

707   Palacios, D., García-Ruiz, J. M., Andrés, N., Schimmelpfennig, I., Campos, N., Léanni, L.,
708   Aumaître, G., Bourlès, D. L. and Keddadouche, K.: Deglaciation in the central Pyrenees during
709   the Pleistocene–Holocene transition: Timing and geomorphological significance, Quaternary
710   Science Reviews, 162, 111–127, doi:10.1016/j.quascirev.2017.03.007, 2017.

711   Pey, J., Pérez, N., Cortés, J., Alastuey, A. and Querol, X.: Chemical fingerprint and impact of
712   shipping emissions over a western Mediterranean metropolis: Primary and aged contributions,
713   Science of The Total Environment, 463–464, 497–507, doi:10.1016/j.scitotenv.2013.06.061,
714   2013.

715   Pey, J., Larrasoaña, J. C., Pérez, N., Cerro, J. C., Castillo, S., Tobar, M. L., de Vergara, A.,
716   Vázquez, I., Reyes, J., Mata, M. P., Mochales, T., Orellana, J. M. and Causapé, J.:
717   Phenomenology and geographical gradients of atmospheric deposition in southwestern
718   Europe: Results from a multi-site monitoring network, Science of The Total Environment, 744,
719   140745, doi:10.1016/j.scitotenv.2020.140745, 2020.

720   Pohjola, V. A., Moore, J. C., Isaksson, E., Jauhiainen, T., Wal, R. S. W. van de, Martma, T.,
721   Meijer, H. a. J. and Vaikmäe, R.: Effect of periodic melting on geochemical and isotopic signals
722   in an ice core from Lomonosovfonna, Svalbard, Journal of Geophysical Research: Atmospheres,
723   107(D4), ACL 1-1-ACL 1-14, doi:10.1029/2000JD000149, 2002.

724   Preunkert, S., McConnell, J. R., Hoffmann, H., Legrand, M., Wilson, A. I., Eckhardt, S., Stohl, A.,
725   Chellman, N. J., Arienzo, M. M. and Friedrich, R.: Lead and Antimony in Basal Ice From Col du
726   Dome (French Alps) Dated With Radiocarbon: A Record of Pollution During Antiquity,
727   Geophysical Research Letters, 46(9), 4953–4961, doi:10.1029/2019GL082641, 2019.

728 Querol, X., Viana, M., Alastuey, A., Amato, F., Moreno, T., Castillo, S., Pey, J., de la Rosa, J.,
729 Sánchez de la Campa, A., Artíñano, B., Salvador, P., García Dos Santos, S., Fernández-Patier, R.,
730 Moreno-Grau, S., Negral, L., Minguillón, M. C., Monfort, E., Gil, J. I., Inza, A., Ortega, L. A.,
731 Santamaría, J. M. and Zabalza, J.: Source origin of trace elements in PM from regional
732 background, urban and industrial sites of Spain, Atmospheric Environment, 41(34), 7219–7231,
733 doi:10.1016/j.atmosenv.2007.05.022, 2007.

734 Reimer, P. J., Bard, E., Bayliss, A., Beck, J. W., Blackwell, P. G., Ramsey, C. B., Buck, C. E., Cheng,
735 H., Edwards, R. L., Friedrich, M. and others: IntCal13 and Marine13 radiocarbon age calibration
736 curves 0–50,000 years cal BP, Radiocarbon, 55(4), 1869–1887, 2013.

737 Rico, I., Izagirre, E., Serrano, E. and López-Moreno, J. I.: Superficie glaciar actual en los Pirineos:
738 Una actualización para 2016, Pirineos, 172(0), 029, doi:10.3989/Pirineos.2017.172004, 2017.

739 Salazar, A., Mata, M. P., Rico, M., Valero-Garcés, Oliva-Urcia, B. and Rubio, F. M.: El paleolago
740 de La Larri (Valle de Pineta, Pirineos), Cuadernos de Investigación Geográfica, 39(1), 97–116,
741 2013.

742 Sanchez-Cabeza, J. A., Masqué, P. and Ani-Ragolta, I.: 210Pb and210Po analysis in sediments
743 and soils by microwave acid digestion, J Radioanal Nucl Chem, 227(1), 19–22,
744 doi:10.1007/BF02386425, 1998.

745 Serrano, E. and Martín-Moreno, R.: Surge glaciers during the Little Ice Age in the Pyrenees,
746 Cuadernos de Investigación Geográfica, 44(1), 213–244, doi:10.18172/cig.3399, 2018.

747 Solomina, O. N., Bradley, R. S., Hodgson, D. A., Ivy-Ochs, S., Jomelli, V., Mackintosh, A. N.,
748 Nesje, A., Owen, L. A., Wanner, H., Wiles, G. C. and Young, N. E.: Holocene glacier fluctuations,
749 Quaternary Science Reviews, 111, 9–34, doi:10.1016/j.quascirev.2014.11.018, 2015.

750 Solomina, O. N., Bradley, R. S., Jomelli, V., Geirsdottir, A., Kaufman, D. S., Koch, J., McKay, N. P.,
751 Masiokas, M., Miller, G., Nesje, A., Nicolussi, K., Owen, L. A., Putnam, A. E., Wanner, H., Wiles,
752 G. and Yang, B.: Glacier fluctuations during the past 2000 years, Quaternary Science Reviews,
753 149, 61–90, doi:10.1016/j.quascirev.2016.04.008, 2016.

754 Taylor, S. R. and McLennan, S. M.: The geochemical evolution of the continental crust, Reviews
755 of Geophysics, 33, 241–265, 1995.

756 Uglietti, C., Zapf, A., Jenk, T. M., Sigl, M., Szidat, S., Salazar, G. and Schwikowski, M.:
757 Radiocarbon dating of glacier ice: overview, optimisation, validation and potential, The
758 Cryosphere, 10(6), 3091–3105, doi:10.5194/tc-10-3091-2016, 2016.

759 Wanner, H., Solomina, O., Grosjean, M., Ritz, S. P. and Jetel, M.: Structure and origin of
760 Holocene cold events, Quaternary Science Reviews, 30(21–22), 3109–3123,
761 doi:10.1016/j.quascirev.2011.07.010, 2011.

762 Zemp, M., Frey, H., Gärtner-Roer, I., Nussbaumer, S. U., Hoelzle, M., Paul, F., Haeberli, W.,
763 Denzinger, F., Ahlstrøm, A. P., Anderson, B., Bajracharya, S., Baroni, C., Braun, L. N., Cáceres, B.
764 E., Casassa, G., Cobos, G., Dávila, L. R., Granados, H. D., Demuth, M. N., Espizua, L., Fischer, A.,
765 Fujita, K., Gadek, B., Ghazanfar, A., Hagen, J. O., Holmlund, P., Karimi, N., Li, Z., Pelto, M., Pitte,
766 P., Popovnin, V. V., Portocarrero, C. A., Prinz, R., Sangewar, C. V., Severskiy, I., Sigurđsson, O.,
767 Soruco, A., Usubaliev, R. and Vincent, C.: Historically unprecedented global glacier decline in
768 the early 21st century, Journal of Glaciology, 61(228), 745–762, doi:10.3189/2015JoG15J017,
769 2015.

770   Zemp, M., Huss, M., Thibert, E., Eckert, N., McNabb, R., Huber, J., Barandun, M., Machguth, H.,
771   Nussbaumer, S. U., Gärtner-Roer, I., Thomson, L., Paul, F., Maussion, F., Kutuzov, S. and Cogley,
772   J. G.: Global glacier mass changes and their contributions to sea-level rise from 1961 to 2016,
773   Nature, 568(7752), 382–386, doi:10.1038/s41586-019-1071-0, 2019.

774
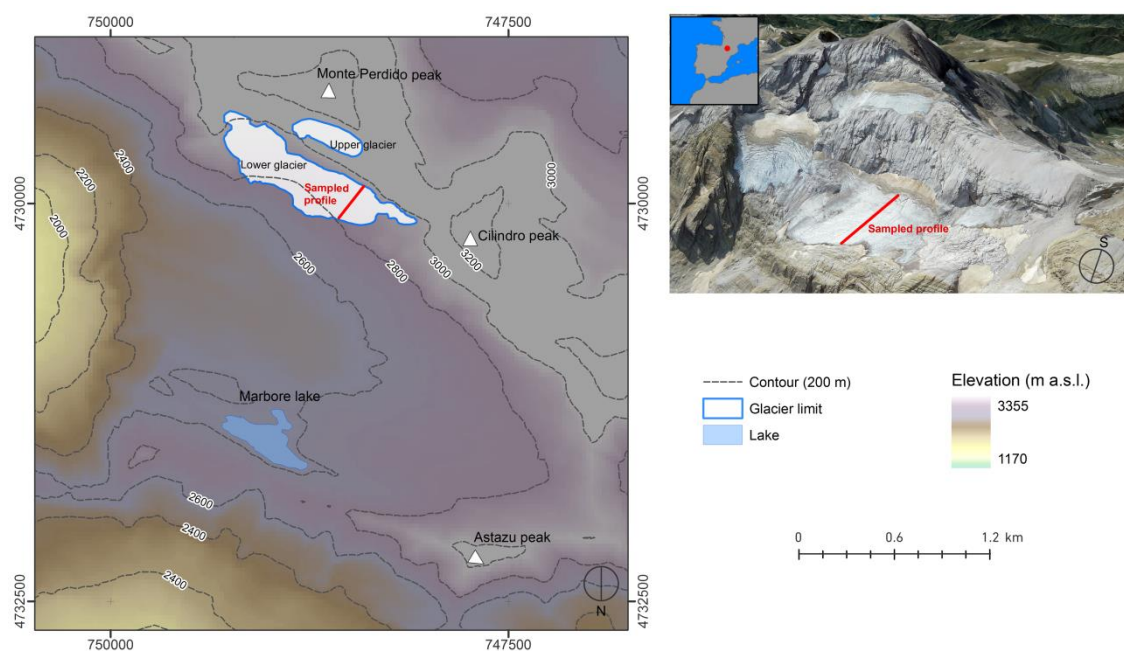
Figure 1. (left) Location of Monte Perdido Glacier (MPG) within a digital elevation map of Marboré Cirque; (right) Picture (©Google Earth) of MPG where the location of the sampled profile is indicated (see Fig. 2).

782
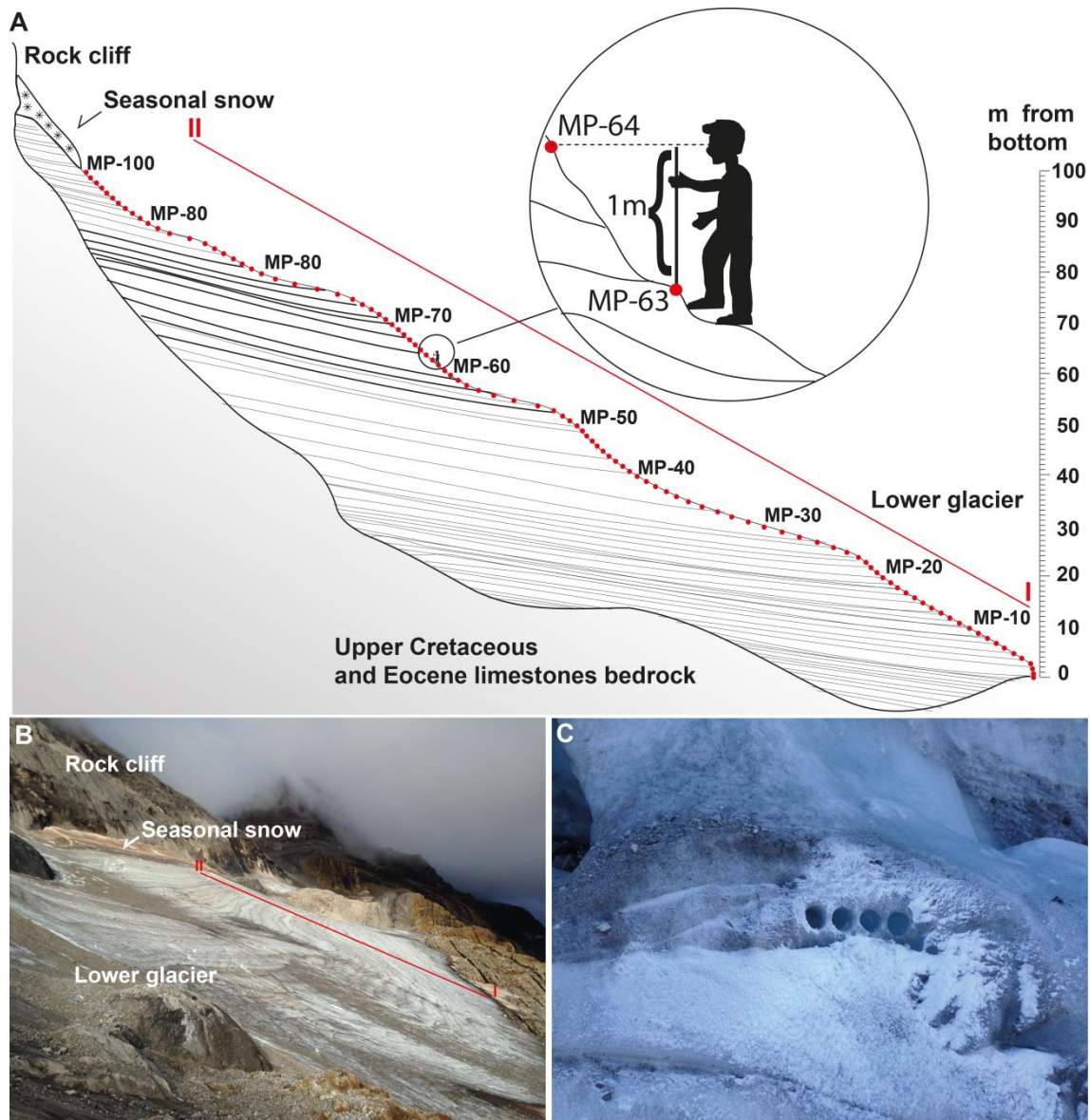
783 **Figure 2**. (A) Simplified scheme with the position of the 100 samples collected along

784 the slope (red line I-II marks the profile indicated in B; identification of the samples is

785 MP-0 to MP-100). According to the ice bedding (tilt is approximate) the oldest material

786 should be found at the bottom of the lower glacier. Note the inset with a detailed view

787 of the sampling procedure measuring a height difference of 1 m to obtain every

788 sample. (B) Image of the Monte Perdido glacier surface where the sampling was

789 carried out (red line I- II represents the sampled profile shown in Figure 1). Note the

790 presence of dark debris-rich layers alternating with cleaner ice. (C). Detailed view

791 indicating that every sample consisted in 3-4 small horizontally-drilled cylinders (see

792 text for more details).

793

794

795
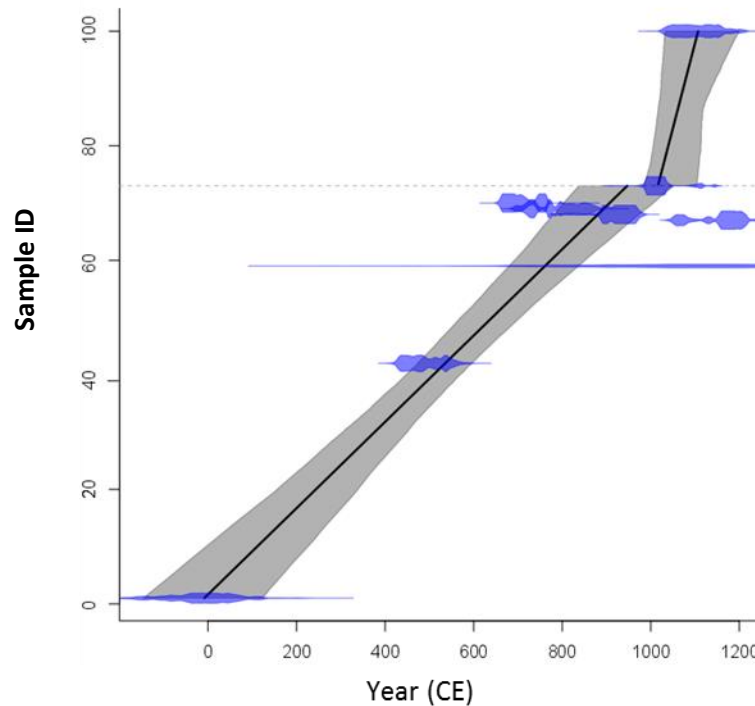
Figure 3. Age model for the Monte Perdido ice sequence based on linear interpolation of ^{14}C data (Table 3), obtained using the Clam software (Blaauw, 2010; Blaauw et al., 2019). Y axis indicates the number of samples from MP-0 to MP-100 (see Fig. 2). The dates appear as the calendar-age probability distributions in blue, while the black line is the resulting depth-age model and the gray envelope shows the 95 % confidence interval. Note the hiatus located at 73 m indicated by a dashed line. The error of sample MP59m is so high that appears as a horizontal line.

803
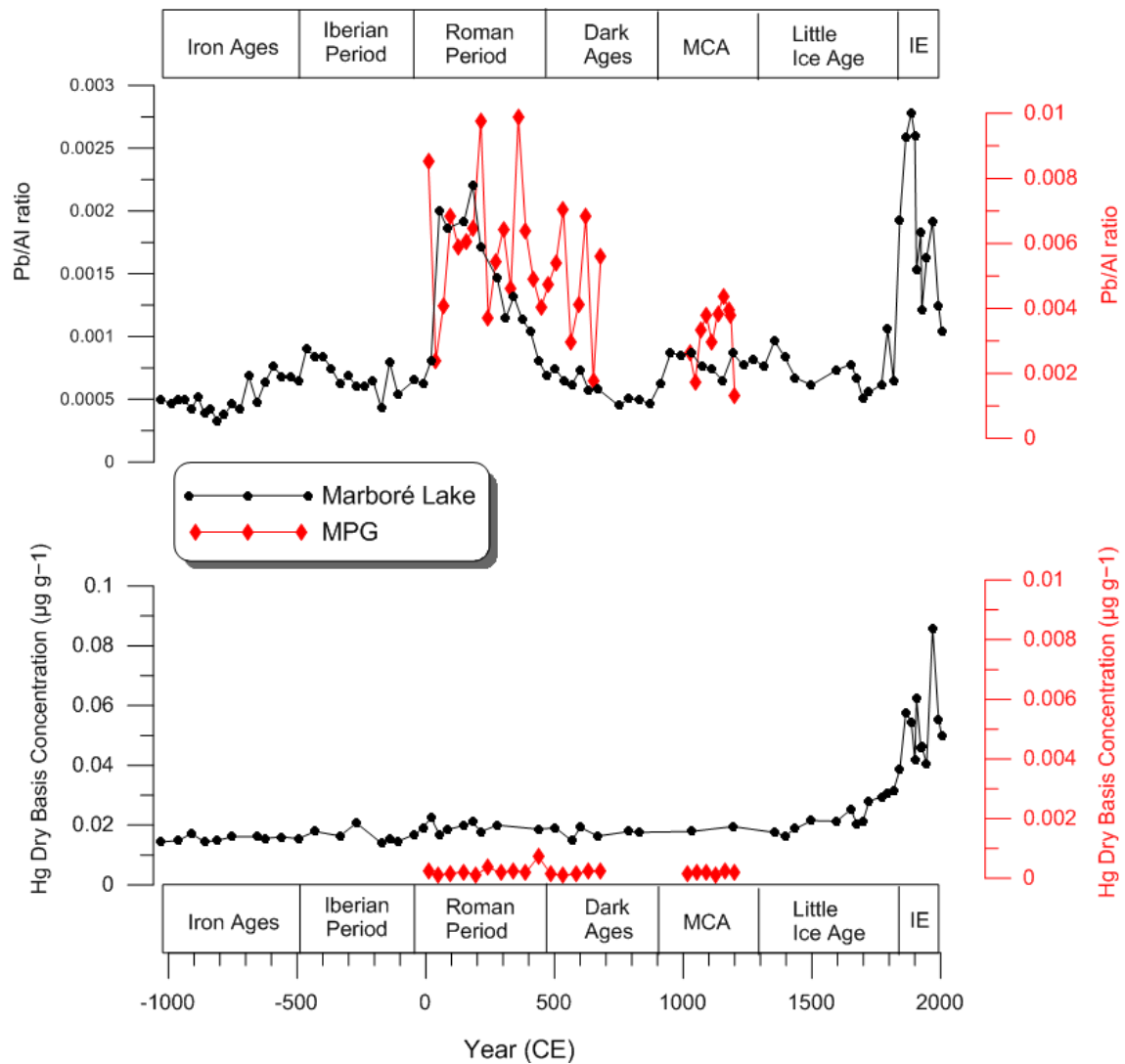
804
805 **Figure 4.** Comparison of Pb/Al ratio and Hg concentration of dry weight sediment in

806 MPG samples with data obtained from Marboré Lake sediments (Corella et al., 2021).

807 Note the differences in the vertical axis.

808

809

810
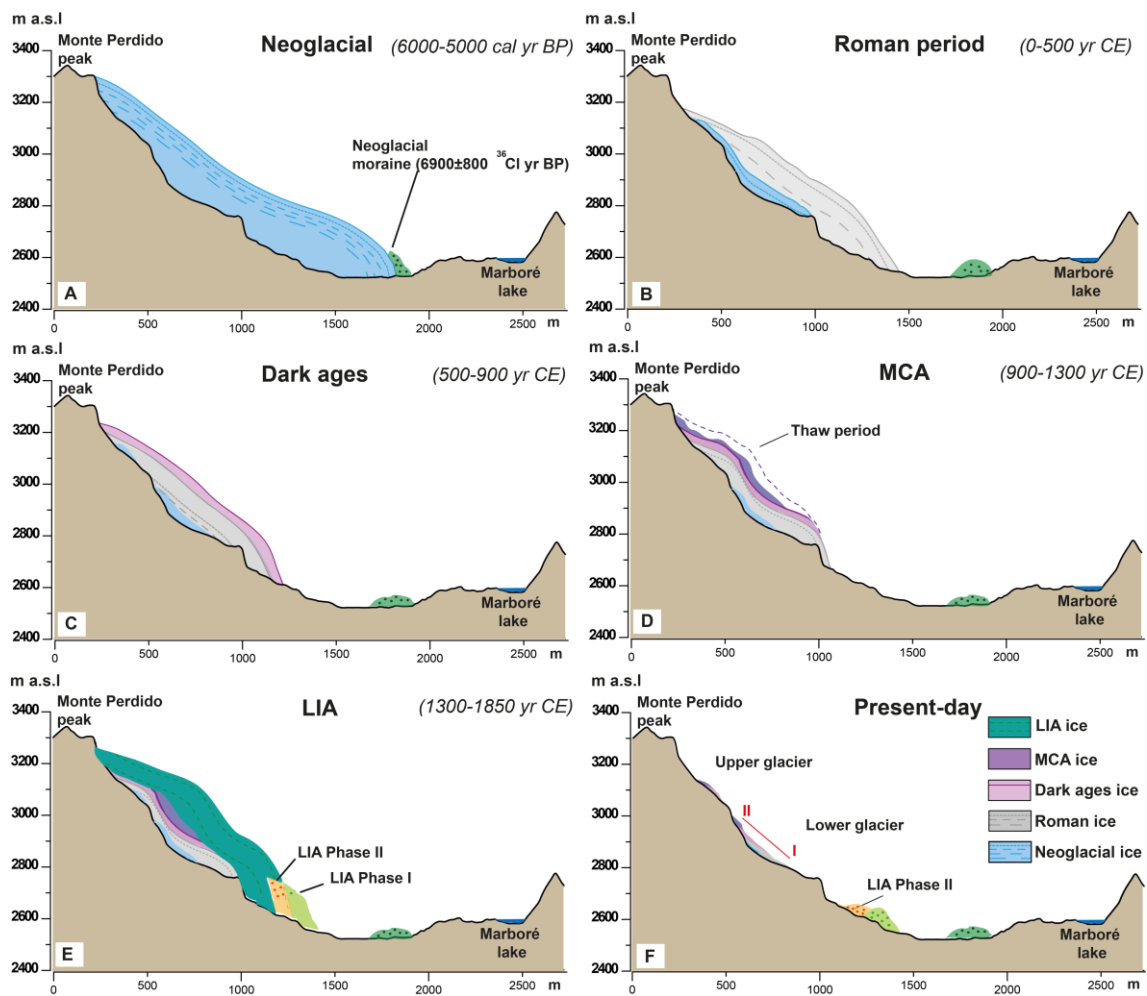
Figure 5. Geomorphic transects (south to north) taken from the Marboré Cirque, showing the tentative reconstruction of MPG during the six main stages discussed in the text. A) Neoglacial Period (ca. 5000 – 6000 cal yr BP) where the Neoglacial moraine is indicated (García-Ruiz et al., 2014); (B) Roman Period (0-500 CE) when the glacier is shown considerably retreated; (C) Dark Ages (500-900 CE); (D) Medieval Climate Anomaly (900-1300 CE), a period when the glacier retreated and ablation caused a concentration of debris and organic remains form dark layers in the glacier ice (discontinuous line aims to highlight the importance of melting processes); (E) Little Ice Age (1300-1850 CE), with the MPG reaching the LIA moraines position and (F) present-day situation characterized by the MPG divided into two ice bodies, no ice remaining from the LIA, and very steep slopes (sampling transect indicated by a red line).

822 **Table 1.** Concentrations of ^{137}Cs in the soluble water fraction of ice from Monte

823 Perdido samples.

Sample	Mass of ice analyzed (g)	MDA (Bq·L^{-1})
MP-61	240	0.15
MP-82	178	0.16
MP-97	232	0.14
MP-98	376	0.09
MP-100	238	0.17

824

825 **Table 2.** Determination of ^{210}Pb activity in the soluble water fraction of 100 g of ice

826 from Monte Perdido samples.

Sample	^{210}Pb activity (Bq·L^{-1})	MDA (Bq·L^{-1})
MP-73	17.4 ± 2.6	1.14
MP-76	6.2 ± 1.3	0.70
MP-82	<MDA	0.61
MP-85	<MDA	0.84
MP-88	<MDA	1.23
MP-91	<MDA	1.05
MP-94	<MDA	0.71
MP-97	<MDA	0.77
MP98	<MDA	0.58
MP-100	8.5 ± 1.5	0.71

827

828

Table 3. Radiocarbon dating of MPG samples indicating their origin, the radiocarbon age (^{14}C age BP) and the calibrated date using INTCAL13 curve and presented in calendar years Common Era (CE). Samples in red and *italics* were not included in the age model (see column "comments" and text for explanation).

Sample origin	Sample ID	Laboratory ID	^{14}C age BP	Cal age (CE)	Comments
Bulk organic matter	MP-1	D-AMS 025291	2000±64	8±66	Used in the age model
	MP-42	D-AMS 025294	1554±27	462±32	Used in the age model
	MP-48	D-AMS 025295	73±33	*1897±20*	*Discarded due to plastic contamination*
	MP-67	D-AMS 025296	876±29	1185±31	Used in the age model
	MP-68	D-AMS 026592	1128±22	942±24	Used in the age model
	MP-69	D-AMS 026593	1230±23	730±14	Used in the age model
	MP-70	D-AMS 025297	1308±28	680±16	Used in the age model
	MP-73	D-AMS 025298	1011±25	1012±16	Used in the age model
	MP-100	D-AMS 025299	923±39	1074±31	Used in the age model
Bulk material (filter)	MP-67filter	D-AMS 029894	485±40	*1429±15*	*Discarded due to mixing with detrital fraction*
	MP-81filter	D-AMS 033972	1758±25	*287±68*	
WIOC	MP10m	MP10m	812±755	*854±721*	*Discarded due to too high error*
	MP59m	MP59m	926±268	1046±242	Used in the age model
Pollen concentration	MP-30pollen	D-AMS 031464	3906±42	*-2384±1332*	*Discarded due to technical issues and too high errors*
	MP-70pollen	D-AMS 031465	1787±37	*237±255*	
	MP-100pollen	D-AMS 031466	1854±30	*158±807*	

834 **Table 4.** Elemental concentration (ppm) of major and trace metals in both Ordesa's

835 current deposited dust and MPG ice deposits (averaged values for the 35 analyzed

836 samples), as well as Upper Crust (UC) elemental contents for comparison (Taylor and

837 McLennan, 1995). On the right side, Al-normalised Enrichment Factors (EF) for dust

838 components and elements for: EF_i, the MPG ice dust versus the current Ordesa's

839 deposited dust (CODD); EF_{iCODD}, the CODD versus the UC; and EF_{iMPGID}, the MPG ice

840 dust versus the UC. Numbers in bold type in the EF represent anomalous values

841 (elements enriched in Ordesa samples or in MPG ones).

	Ordesa 2016-2017 (2-year atmospheric deposition)			Monte Perdido (ice dust: 35 filter samples)			Upper Crust	Al-Normalised Enrichment Factors		
	Max	Min (ppm)	Average	Max	Min (ppm)	Average	(ppm)	EF_i	EF_{iCODD}	EF_{iMPGID}
OC	443270	49659	206814	436343	14793	126381		0,4		
EC	114519	12506	39995	112769	14668	40605		0,6		
Al	122401	7883	60410	506467	19611	98808	80400	1,0	1,0	1,0
Ca	22578	3182	9663	119648	256,7	11984	30000	0,8	0,4	0,3
Fe	63218	2901	32665	183957	12504	59477	35000	1,1	1,2	1,4
K	27478	3907	14839	57038	4001	18505	28000	0,8	0,7	0,5
Mg	27286	2105	12265	72210	3513	16645	13300	0,8	1,2	1,0
Na	5380	1,2	1413	25750	593	5126	28900	2,2	0,1	0,1
Ti	5035	257	2334	52192	3243	13662	3000	**3,6**	1,0	**3,7**
Mn	1656	128	582	3835	174	979	600	1,0	1,3	1,3
Sr	170	19	78	200	20	80	350	0,6	0,3	0,2
Be	7	0	2,1	2,3	0	0,4	3	0,1	0,9	0,1
V	208	10	76	257	28	107	60	0,9	1,7	1,5
Cr	720	5	118	2915	12	441	35	**2,3**	**4,5**	**10,3**
Co	32	0	7,6	49	5,4	20	10	1,6	1,0	1,6
Ni	414	7	55	1046	4,3	228	20	**2,5**	**3,6**	**9,3**
Cu	683	33	127	26451	92	3786	25	**18,3**	**6,7**	**123,2**
Zn	9391	164	1316	3826	171	988	71	0,5	**24,7**	**11,3**
As	26	2	10	51	5,3	18	1,5	1,0	**9,1**	**9,6**
Se	90	0	22	30	0	5,2	50	0,1	0,6	0,1
Cd	100	0	14	1,5	0	0,3	0,98	0,0	**18,8**	0,2
Sb	26	0	4,5	59	2	11	0,2	1,5	**29,7**	**43,3**
Ba	1010	15	287	870	67	317	550	0,7	0,7	0,5
Tl	1	0	0,1	1,1	0	0,2	0,75	1,7	0,1	0,2
Pb	175	8	53	2989	86	495	17	**5,7**	**4,2**	**23,7**
Th	37	1	12	26	1,6	9,7	10,7	0,5	1,5	0,7
U	8	0	2,5	15	0	3,7	2,8	0,9	1,2	1,1

842